Japanese Journal of Applied Physics **64**, 110803 (2025) **PROGRESS REVIEW**
https://doi.org/**10.35848/1347-4065/ae1842**

Structure and electronic properties of RuSi, OsSi, RhSi, ReSi and IrSi

Dmitri B. Migas[1,2*], Andrew B. Filonov[1], Nikolay G. Galkin[3], and Natalia V. Skorodumova[4]

[1]*Belarusian State University of Informatics and Radioelectronics, P. Browki 6, 220013 Minsk, Belarus*
[2]*National Research Nuclear University MEPhI (Moscow Engineering Physics Institute), Kashirskoe shosse 31, 115409, Moscow, Russia*
[3]*Institute of Automation and Control Processes FEB RAS, 690041 Vladivostok, 5, Radio Str., Russia*
[4]*Applied Physics, Division of Materials Science, Department of Engineering Sciences and Mathematics, Luleå University of Technology, Luleå SE-97187, Sweden*

[*]E-mail: migas@bsuir.by

Received September 12, 2025; revised October 22, 2025; accepted October 28, 2025; published online November 12, 2025

RuSi, OsSi, RhSi, ReSi and IrSi in different phases have been investigated by means of ab initio techniques within the hybrid functional. RuSi and OsSi have the cubic (space group $P2_13$, #198) structure and display semiconducting properties, while the conducting high-temperature cubic phase (space group Pm3m, #221) is sizably higher in energy. The ground state for RhSi and IrSi is the orthorhombic (space group Pnma, #62) structure, while for ReSi it is monoclinic (space group $P2_1/c$, #14) with the cubic phase (space group $P2_13$, #198) to be higher in total energy. The Dirac nodes and cones as well as crossing bands with linear dispersion are found for RhSi, ReSi and IrSi in the orthorhombic phase. These monosilicides in the monoclinic phase can be viewed as gapless semiconductors except for IrSi with the band gap of 0.23 eV.

1. Introduction

Monosilicides CrSi, MnSi, FeSi, CoSi, RuSi, OsSi, RhSi and ReSi crystalize in the cubic structure (space group $P2_13$, #198) displaying a variety of properties.[1,2)] CrSi is a paramagnetic metallic material with low resistivity[3)] having holes as main carriers.[4,5)] Additionally, a large positive magnetoresistance and competing ferromagnetic and antiferromagnetic correlations have also been reported for this material.[4)] MnSi s a chiral helimagnetic material and characterizes by interesting magnetic properties originated from a magnetic skyrmion state due to the Dzyaloshinskii–Moriya interaction of Mn magnetic moments in a spiral way.[6,7)] In the case of FeSi, a metal–insulator transition from a narrow-gap semiconductor (0.05–0.1 eV as estimated from resistivity and optical measurements) to a weak metal is revealed at about 200 K.[8–11)] CoSi and RhSi can be viewed as chiral Weyl semimetals with topological non-trivial electronic states hosting unconventional multifold Fermions.[12–17)] RuSi and OsSi are semiconductors with the experimentally determined band gaps of 0.2–0.4 eV.[18–21)] At the same time little is known about the properties of ReSi due to its peritectic formation in a narrow temperature range of ∼1680 °C–1880 °C.[22)]

Ab initio calculations performed for CrSi within the local density and generalized gradient approximations revealed conducting properties since the Fermi level crossed some bands.[23,24)] The features in the band structure of MnSi were traced by means of density functional theory paired with dynamical mean-field theory to treat a highly correlated system indicating the multi-sheet Fermi surface and the appearance of small magnetic moments on Mn atoms.[25)] Nonmagnetic FeSi, RuSi and OsSi were intensively investigated by different ab initio techniques within the local density or generalized gradient approximation and also involving modified Becke–Johnson exchange potential[26–33)] demonstrating the indirect band-gap nature of these compounds in addition to the loops of extrema both in the valence and conduction bands near the Γ point.[26)] Moreover, the corresponding bad-gap values were estimated in the range of 0.13–0.38 eV, 0.21–0.48 eV and 0.33–0.74 eV for FeSi, RuSi and OsSi, respectively.[26–33)] CoSi and RhSi were found to have a threefold degeneracy at the Γ point near the Fermi level leading to a threefold fermion[34)] as determined by results of ab initio calculations and high-resolution angle-resolved photoemission spectroscopy. ReSi can be considered both as a metal and as a degenerate semiconductor because the Fermi level crosses some bands ∼1 eV below the gap.[35)]

It should be mentioned here that these monosilicides are characterized not only by the cubic structure (space group $P2_13$, #198). In fact, a monoclinic lattice (space group $P2_1$, #4), being structurally very close to the cubic one, has been recently theoretically predicted by means of ab initio calculations with a hybrid functional and experimentally confirmed by high-resolution transmission electron microscopy to be the ground state of CrSi[36,37)] and FeSi.[38)] The appearance of the monoclinic phase of CrSi and FeSi could help in explaining holes as the main charge carriers for CrSi due to some features in band dispersion near the Fermi level[36)] and shed some light on the metal–insulator transition for FeSi since the cubic and monoclinic phases are semiconducting and conducting, respectively,[38)] in addition to some issues connected to the appearance of the magnetic ordering.[37,38)] In the case of RuSi and OsSi another cubic phase (space group Pm3m, #221) has been found (known as a high temperature phase[18,39–45)]) in which these monosilicides are conductors.[40–45)] RhSi can also have an orthorhombic structure (space group Pnma, #62)[39,46)] and display a symmetry-protected Dirac nodal line and symmetry-enforced Dirac nodes.[47)] Moreover, RhSi in a monoclinic phase (space group $P2_1/c$, #14) is reported to exist[39,48)] but there is no information on properties of this phase.

The aim of this paper is to trace changes in the total energies of RuSi, OsSi, RhSi and ReSi in different phases and in their band structures primarily focusing on the issues related to Dirac and Weyl features by applying ab initio

techniques within a hybrid functional. In addition, IrSi in cubic and monoclinic phases are considered in comparison with the orthorhombic ground state.

2. Details of calculations

The full structural optimization (both lattice parameters and atomic positions) followed by band-structure calculations for RuSi, OsSi, RhSi, ReSi and IrSi in different phases were performed by the first principles total energy projector-augmented wave method (code VASP)[49–52] within the screened hybrid functional of Heyd, Scuseria, and Ernzerhof (HSE) known as HSE06[53–56] with the standard settings for the screening and Hartree–Fock mixing parameters (the 0.25 fraction of the exact exchange). The energy cutoff was set to 350 eV for all compounds. For the self-consistent procedure fine meshes of Monkhorst–Park points were implemented: $13 \times 13 \times 13$ for the cubic (space group Pm3m, #221) phase, $9 \times 9 \times 9$ for the cubic (space group $P2_13$, #198) phase, $7 \times 7 \times 7$ for the monoclinic (space group $P2_1$, #4) phase, $7 \times 7 \times 7$ for the monoclinic (space group $P2_1/c$, #14) phase and $7 \times 9 \times 5$ for the orthorhombic (space group Pnma, #62) phase to reach the convergence of the total energy less than 0.001 eV per formula unit. The atomic relaxation was stopped when the forces acting on atoms became smaller than 0.001 eV $Å^{-1}$. The total density of states was calculated by implementing the tetrahedron method with Blöchl corrections.

3. Results and discussion

The unit cells of RuSi, OsSi, RhSi, ReSi and IrSi in different phases (namely, cubic with space groups $P2_13$, #198 and Pm3m, #221, orthorhombic with space group Pnma, #62, monoclinic with space group $P2_1/c$, #14) are shown in Fig. 1. It should be noted here that after the full structural optimization all these monosilicides in the monoclinic crystal structure (space group $P2_1$, #4) converged to the cubic one (space groups $P2_13$, #198). This issue can be explained by the fact that RuSi, OsSi, RhSi, ReSi and IrSi are nonmagnetic materials, while the monoclinic $P2_1$, #4 crystal structure is typical of CrSi and FeSi exhibiting the antiferromagnetic ordering.[36–38] There is rather good agreement between the calculated lattice parameters and experimentally determined ones (Table I). In general, the theoretically estimated lattice parameters are slightly smaller than the experimental ones. But if one makes a correction for the thermal expansion coefficient (usually experimental data are obtained at room temperature whereas theoretical estimates at zero temperature) for these monosilicides the agreement becomes even better.

The other issue worthwhile to be discussed is a difference in the total energy of various phases of RuSi, OsSi, RhSi, ReSi and IrSi (Table II). For RuSi and OsSi it is evident that the cubic $P2_13$, #198 phase is the ground state followed by the cubic Pm3m, #221 phase (high-temperature phase[39–45]) while the orthorhombic Pnma, #62 and monoclinic $P2_1/c$, #14 phases are sizably higher in energy. For RhSi the orthorhombic Pnma, #62 is the ground state followed by the monoclinic $P2_1/c$, #14 phase, which is turned out to be more stable than the cubic $P2_13$, #198 one, while the cubic Pm3m, #221 phase is higher in energy. Our results indicate that the appearance of RhSi in the monoclinic structure should not come as a surprise. In the case of ReSi we have found the monoclinic $P2_1/c$, #14 phase to be the ground state while the orthorhombic Pnma, #62 one is just slightly higher in energy. From the other side, the cubic $P2_13$, #198 phase of ReSi is the least stable one. It is not excluded that ReSi in the orthorhombic and monoclinic phases could be formed as ultrathin films and precipitates stabilized by low interface energy with a substrate, while a bulk-like form of ReSi can exist at high temperatures.[22] The ground state for IrSi is confirmed to be the orthorhombic Pnma, #62 phase followed by the monoclinic $P2_1/c$, #14 phase. It is possible that the metastable monoclinic phase of IrSi could also be stabilized in the form of ultrathin films and precipitates. IrSi in any of the cubic phases is clearly higher in energy. The full structural optimization also revealed that the variation in the interatomic distances of the first neighbors (between metal and silicon atoms) differs differently for RuSi, OsSi, RhSi, ReSi and IrSi having the same structure (Table II). This is more pronounced for the orthorhombic, monoclinic and cubic cubic $P2_13$, #198 phases and can affect electronic properties of these monoslicides.

For all the investigated monosilicides we did not find the appearance of magnetic moments on metal atoms indicating nonmagnetic ordering. RuSi and OsSi in the cubic $P2_13$, #198 phase display semiconducting properties (see Fig. 2) in accordance with the experimental data.[18–21] The band dispersion with multiple extrema both in the top valence band and in the bottom of the conduction band (along Γ–R, Γ–X, Γ–M) forming loops of extrema are evident being in prefect agreement with previous theoretical results.[26–33] Such loops of extrema are not unique for silicides. They were previously observed for Ca_3Si_4.[59] The hybrid functional sizably overestimates the band gaps (0.78 eV for RuSi and 1.17 eV for OsSi) as compared to the experimentally determined ones of 0.2–0.4 eV.[18–21] This issue is also typical of isostructural FeSi[38] and quasi-particle calculations within the GW approximation are necessary to provide a reasonable comparison with the experimental data.

For the cubic Pm3m, #221 phase we confirm the conducting properties[40–45] because the Fermi level crosses some bands (Fig. 2). The most striking feature in the band topology is the appearance of linear band dispersion with crossing bands at $0.5 \times$ R–M just 0.3 eV (for RuSi) and 0.4 eV (for OsSi) below the Fermi level. It is not excluded that the Dirac cone is formed here that requires further investigation.

The band structures of RhSi and IrSi in the cubic $P2_13$, #198 phase (which can be viewed as chiral Weyl semimetals) display a threefold degeneracy at the Γ point near the Fermi level, while cubic ReSi does not possess similar band dispersion displaying instead *p*-type degenerate semiconducting properties (Fig. 3). A detailed view of the topological features in the band dispersion near the Γ point is shown in Fig. 4. The calculated band structures are similar to those presented in Refs. 34, 35, 60.

RhSi, ReSi and IrSi in the orthorhombic Pnma, #62 phase are characterized by conducting properties. Moreover, several specific peculiarities in their band structures such as Dirac nodes, cones and crossing bands at various k-points of the Brillouin zone can be spotted near the Fermi energy. In fact, the features at the S, R, Y points for all these

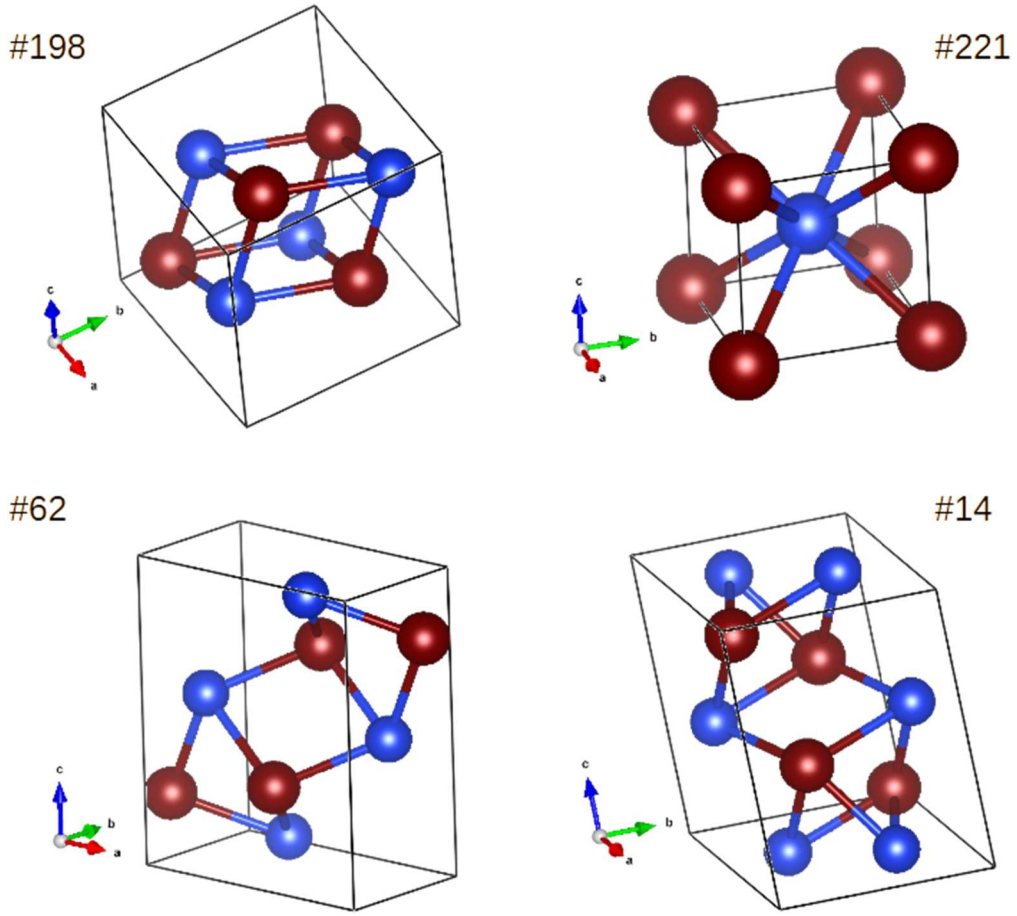

Fig. 1. Crystal structures (unit cells) of different phases of RuSi, OsSi, RhSi, ReSi and IrSi. The corresponding numbers of space groups and crystallographic axes are indicated. Large, brown spheres stand for metal atoms while small, blue spheres—for silicon atoms.

Table I. Comparison between theoretical results (this work) and experimental data on the lattice parameters of RuSi, OsSi, RhSi, ReSi and IrSi in different phases.

		Phase	*a* (Å)	*b* (Å)	*c* (Å)	β
RuSi	Theory	#198	4.6792	—	—	—
	Experiment[39]		4.7006	—	—	—
	Theory	#221	2.9014	—	—	—
	Experiment[39]		2.9125	—	—	—
OsSi	Theory	#198	4.73652	—	—	—
	Experiment[39]		4.72769	—	—	—
	Theory	#221	2.9267	—	—	—
	Experiment[57]		2.96	—	—	—
RhSi	Theory	#198	4.66115	—	—	—
	Experiment[39]		4.67638	—	—	—
	Theory	#62	5.52644	3.04320	6.38149	—
	Experiment[39]		5.5526	3.06894	6.3740	—
	Theory	#14	4.56937	4.54233	5.52156	115.63°
	Experiment[39]		4.5892	4.5728	5.5241	116.214°
ReSi	Theory	#198	4.75138	—	—	—
	Experiment[58]		4.775	—	—	—
IrSi	Theory	#62	5.56765	3.14216	6.37435	—
	Experiment[39]		5.5460	3.21505	6.2576	—

monosilicides in addition to the ones at $0.5 \times \Gamma$–Y direction (for RhSi and IrSi) and at $0.5 \times$ X–Γ (for ReSi) should be further investigated in detail to clarify the exact nature of these peculiarities. It should be noted that similar features were earlier observed for the orthorhombic rhodium[47] and iridium[61] monosilicides.

RhSi, ReSi and IrSi in the monoclinic $P2_1/c$, #14 phase do not have any feature related to the linear band dispersion near the Fermi level (Figs. 2 and 3). RhSi and ReSi can be viewed as gapless semiconductors with holes as main charge carries since the Fermi level mostly stays in the valence band, while the gap of 0.23 eV is found for IrSi. To assure

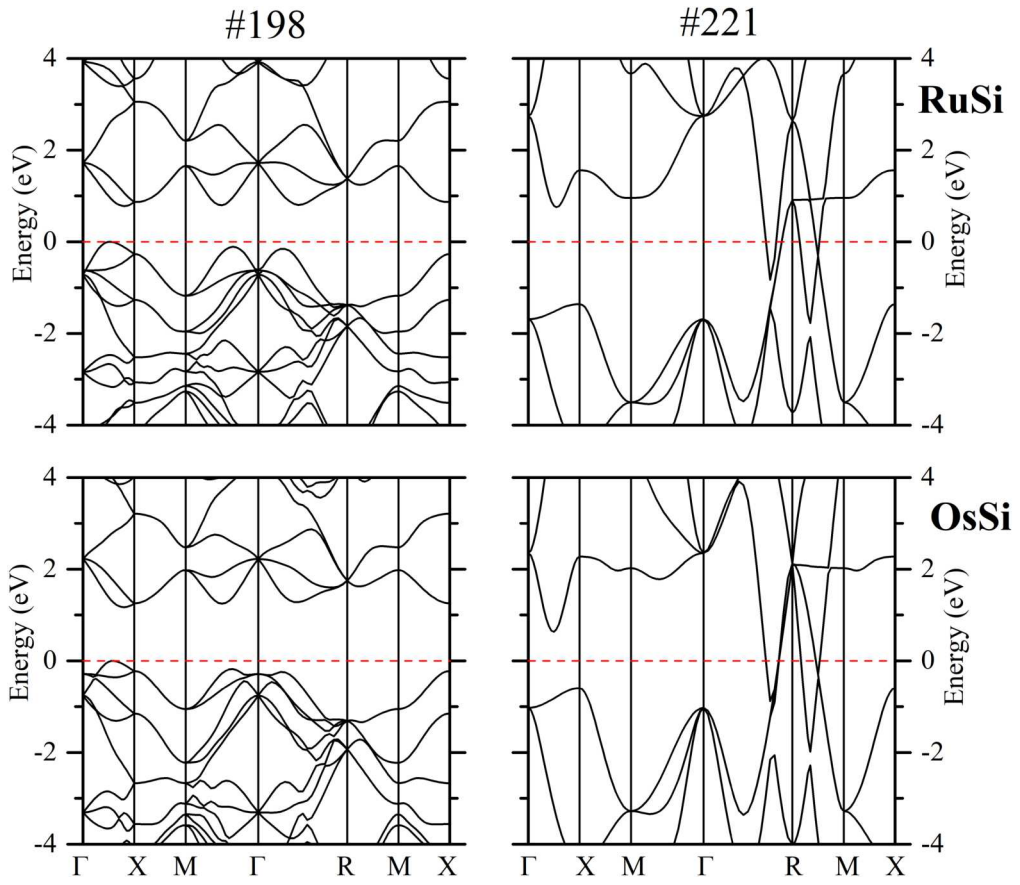

Fig. 2. Band structures of RuSi and OsSi in the cubic $P2_13$, #198 and Pm3m, #221 structures. Zero at the energy scale corresponds to the top of the valence band (the cubic $P2_13$, #198 phase) or to the Fermi energy (the cubic Pm3m, #221 phase). The coordinates of the high-symmetry points in the reciprocal space are: Γ (0 0 0), X (0.5 0 0), M (0.5 0.5 0), R (0.5 0.5 0.5).

Table II. Lattice parameters, metal (Me)–silicon interatomic distances, and the differences in the total energy for different phases of RuSi, OsSi, RhSi, ReSi and IrSi.

	Phase	*a* (Å)	*b* (Å)	*c* (Å)	β	Me–Si (Å)	ΔE (eV/f.u.)
RuSi	#198	4.6792	—	—	—	2.36 3 × 2.40 3 × 2.68	0.000
	#14	4.5813	4.5869	5.3667	115.87°	2.41 2.42 2.44 2.48 2.50 2.55	0.224
	#62	5.7506	2.9293	6.2674	—	2 × 2.43 2.44 2 × 2.45 2.46	0.276
	#221	2.9014	—	—	—	8 × 2.51	0.060
OsSi	#198	4.73652	—	—	—	2.36 3 × 2.40 3 × 2.76	0.000
	#14	4.56495	4.59414	5.45664	112.56°	2 × 2.43 2 × 2.47 2.53 2.54	0.124
	#62	5.89206	2.90558	6.29038	—	2 × 2.42 2.45 2 × 2.48 2.55	0.129
	#221	2.9267	—	—	—	8 × 2.53	0.110
RhSi	#198	4.66115	—	—	—	3 × 2.46 2.50 3 × 2.53	0.071
	#14	4.56937	4.54233	5.52156	115.63°	2.38 2.41 2.43 2.45 2.51 2.57	0.030
	#62	5.52644	3.04320	6.38149	—	2 × 2.39 2.40 2.47 2 × 2.50	0.000
	#221	2.9391	—	—	—	8 × 2.55	0.748
ReSi	#198	4.75138	—	—	—	2.38 3 × 2.49 3 × 2.68	0.499
	#14	4.57828	4.63979	5.59878	114.68°	2.43 2.47 2.51 2.52 2.59 2.60	0.000
	#62	5.70092	3.08517	6.33462	—	3 × 2.48 2 × 2.51 2.54	0.069
	#221	2.9587	—	—	—	8 × 2.56	0.340
IrSi	#198	4.72396	—	—	—	3 × 2.47 3 × 2.53 2.68	0.227
	#14	4.62483	4.54318	5.68600	114.01°	2.39 2.42 2.44 2.46 2.52 2.69	0.076
	#62	5.56765	3.14216	6.37435	—	2 × 2.40 2.43 2.47 2 × 2.56	0.000
	#221	2.9795	—	—	—	8 × 2.58	1.083

that we did not miss any band extrema points when calculating the band structure, the total density of states was calculated on a dense mesh of k-points indicating the gap of ∼0.23 eV (see Fig. 5). We also checked how the fraction of the exact exchange in Hartree–Fock mixing affected the gap by changing it from the standard 0.25 down to 0.17, to 0.08, and eventually to 0, since for α-$SrSi_2$ it was shown the fraction of 0.187 to be necessary in order to reproduce the experimentally measured gap.[62] In our case the gap of 0.10 eV is found for the fraction of 0.17, while the band-gap collapse is already observed at the fraction of 0.08. The quasi-particle calculations within the GW approximation

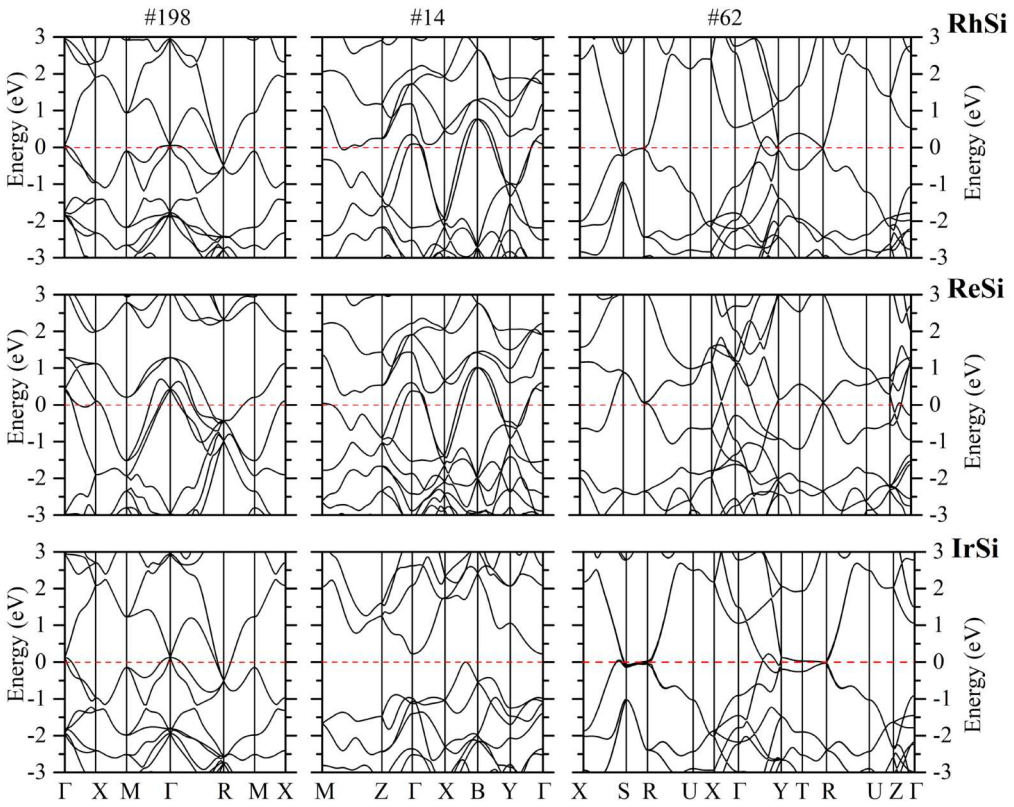

Fig. 3. Band structures of RhSi, ReSi and IrSi in the cubic $P2_13$, #198, monoclinic $P2_1/c$, #14 and orthorhombic Pnma, #62 structures. Zero at the energy scale corresponds to the Fermi energy (except for the IrSi orthorhombic phase where it indicates the top of the valence band). The coordinates of the high-symmetry points in the reciprocal space are: Γ (0 0 0), X (0.5 0 0), M (0.5 0.5 0), R (0.5 0.5 0.5) for the cubic phase, X (0.5 0 0), S (0.5 0.5 0), R (0.5 0.5 0.5), U (0.5 0 0.5), Γ (0 0 0), Y (0 0.5 0), T (0 0.5 0.5), Z (0 0 0.5) for the orthorhombic phase and M (0.5 0.5 0.5), Z (0 0 0.5), Γ (0 0 0), X (0.5 0 0), B (0.5 0.5 0), Y (0 0.5 0) for the monoclinic phase.

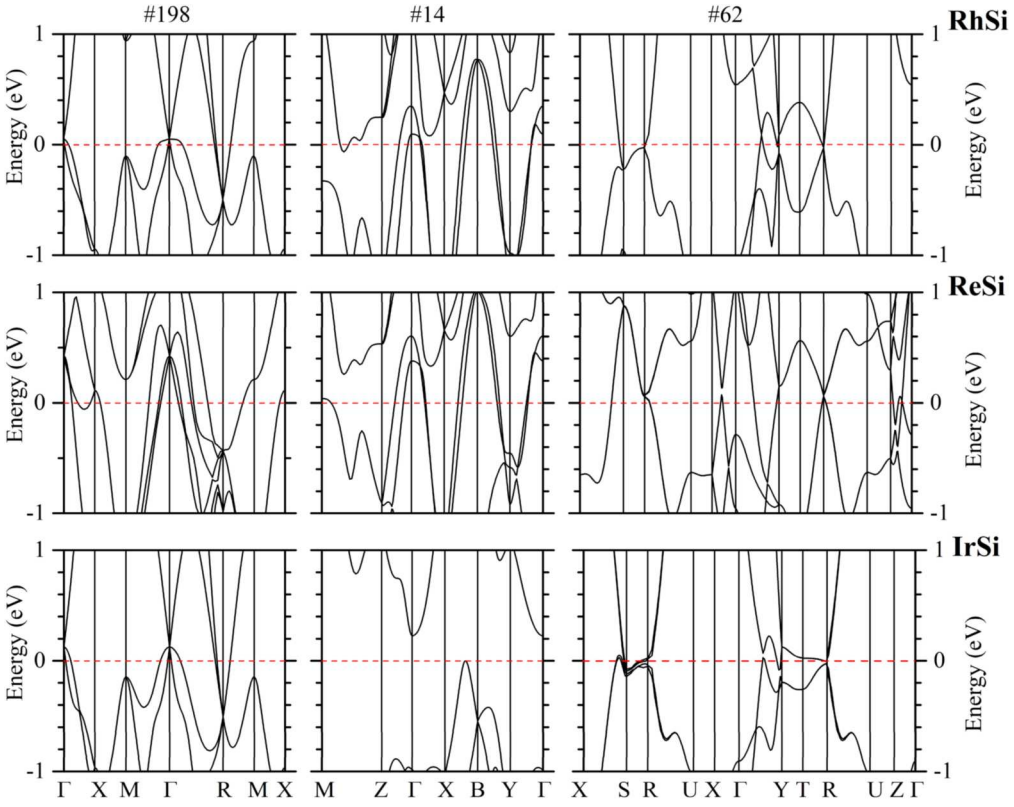

Fig. 4. A detailed view of the band structures of RhSi, ReSi and IrSi in the cubic $P2_13$, #198, monoclinic $P2_1/c$, #14 and orthorhombic Pnma, #62 structures near the Fermi level. Zero at the energy scale corresponds to the Fermi energy (except for the IrSi orthorhombic phase where it indicates the top of the valence band). The coordinates of the high-symmetry points in the reciprocal space are: Γ (0 0 0), X (0.5 0 0), M (0.5 0.5 0), R (0.5 0.5 0.5) for the cubic phase, X (0.5 0 0), S (0.5 0.5 0), R (0.5 0.5 0.5), U (0.5 0 0.5), Γ (0 0 0), Y (0 0.5 0), T (0 0.5 0.5), Z (0 0 0.5) for the orthorhombic phase and M (0.5 0.5 0.5), Z (0 0 0.5), Γ (0 0 0), X (0.5 0 0), B (0.5 0.5 0), Y (0 0.5 0) for the monoclinic phase.

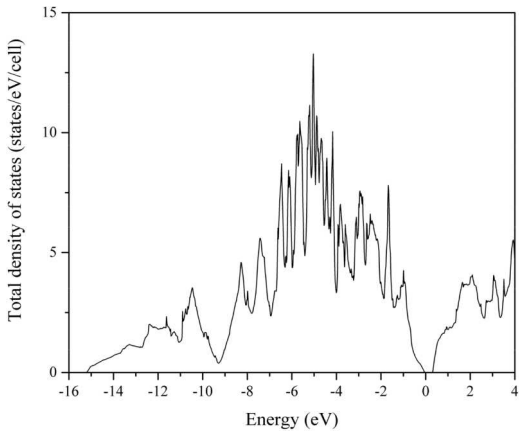

Fig. 5. Total density of states of monoclinic IrSi.

are desirable to assess the band-gap value in monoclinic IrSi. To this end, by taking into account that all considered monosilicides can be viewed as highly correlated systems, at least the onsite Hubbard-U correction should be applied to the d states of metal atoms to investigate electronic properties of these compounds in close comparison with experimental data.

4. Conclusions

We investigated the band structures of RuSi, OsSi, RhSi, ReSi and IrSi in different phases in order to trace features related to the linear band dispersion (Dirac nodes, cones and crossing bands). RuSi and OsSi in the cubic $P2_13$, #198 phase are found to be the ground state. They display semiconducting properties with the loops of extrema in the top valence band and in the bottom conduction band. Their high-temperature cubic Pm3m, #221 phase is higher in total energy and possesses the conducting properties with some crossing bands having the linear band dispersion. We cannot confirm the presence of Dirac cones and this issue requires further investigation. For RhSi, ReSi and IrSi the cubic $P2_13$, #198 phase was revealed to be higher in energy than the monoclinic $P2_1/c$, #14 and orthorhombic Pnma, #62 phases. All monosilicides in the orthorhombic phase contain features in their band structures related to Dirac nodes, cones and crossing bands with the linear dispersion, while the monoclinic phase can be viewed as gapless semiconductors (only for IrSi the appearance of the band gap of 0.23 eV is predicted) without mentioned above topological features. RhSi and IrSi in the cubic $P2_13$, #198 phase are found to have a threefold degeneracy at the Γ point near the Fermi level like in chiral Weyl semimetals contrary to cubic ReSi which is more likely a p-type degenerate semiconductor.

One possible way to modify the properties of the monosilicides is the formation of ternary compounds with two metal atoms having different number of the valence electrons (7—for Re, 8—for Ru and Os, 9—for Rh and Ir). In this case it is feasible to tune the energy position of the Fermi level by moving it closer to the topological features.

The importance of the spin–orbit coupling for the compounds containing 5d elements on the band dispersion can be essential and should be further taken into consideration when studying topological features in the electronic structure of OsSi, ReSi and IrSi.

Acknowledgments

The research was supported by the Belarusian Republican Foundation for Fundamental Research (No. F26RNF-010). The computations were enabled by resources provided by the National Academic Infrastructure for Supercomputing in Sweden (NAISS) at the tetralith supercomputer partially funded by the Swedish Research Council through grant agreement no. 2022-06725. D.B. Migas acknowledges the support from the MEPhI Program Priority 2030.

1) *Semiconducting Silicides*, V. E. Borisenko (ed.) (Springer, Berlin, 2000), Vol. 39, p. 348.
2) *Properties of Metal Silicides*, K. Maex and M. van Rossum (ed.) (Inspec, London, 1995), Vol. 14, p. 335.
3) A. Sakai, S. Yotsuhashi, H. Adachi, F. Ishii, Y. Onose, Y. Tomioka, N. Nagaosa, and Y. Tokura, Int. Conf. Thermoelectrics, 20074569473.
4) S. Banik, M. K. Chattopadhyay, S. Tripathi, R. Rawat, and S. N. Jha, "Large positive magnetoresistance and Dzyaloshinskii–Moriya interaction in CrSi driven by Cr 3d localization," Sci. Rep. **10**, 12030 (2020).
5) N. G. Galkin, A. V. Konchenko, D. L. Goroshko, A. M. Maslov, S. V. Vavanova, and S. I. Kosikov, "Electronic structure, conductivity and carrier mobility in very thin epitaxial CrSi(111) layers with Si(111)$\sqrt{3} \times \sqrt{3}$/30 LEED pattern," Appl. Surf. Sci. **166**, 113 (2000).
6) K. V. Shanavas and S. Satpathy, "Electronic structure and the origin of the Dzyaloshinskii–Moriya interaction in MnSi," Phys. Rev. B **93**, 195101 (2016).
7) F. Freimuth, R. Bamler, Y. Mokrousov, and A. Rosch, "Phase-space Berry phases in chiral magnets: Dzyaloshinskii–Moriya interaction and the charge of skyrmions," Phys. Rev. B **88**, 214409 (2013).
8) P. Samuely, P. Szabó, M. Mihalik, N. Hudáková, and A. A. Menovsky, "Gap formation in Kondo insulator FeSi: point contact spectroscopy," Physica B **218**, 185 (1996).
9) Z. Schlesinger, Z. Fisk, H.-T. Zhang, M. B. Maple, J. F. DiTusa, and G. Aeppli, "Unconventional charge gap formation in FeSi," Phys. Rev. Lett. **71**, 1748 (1993).
10) C. Kloc, E. Arushanov, M. Wendl, H. Hohl, U. Malang, and E. Bucher, "Preparation and properties of FeSi, α-FeSi2, β-FeSi2 single crystals," J. Alloys Compd. **219**, 93 (1995).
11) A. Damascelli, K. Schulte, D. van der Marel, and A. A. Menovsky, "Infrared spectroscopic study of phonons coupled to charge excitations in FeSi," Phys. Rev. B **55**, R4863 (1997).
12) Z. Li, Y. Yuan, R. Hübner, L. Rebohle, Y. Zhou, M. Helm, K. Nielsch, S. Prucnal, and S. Zhou, "B20 weyl semimetal CoSi film fabricated by flash-lamp annealing," ACS Appl. Mater. Interfaces **15**, 30517 (2023).
13) F. M. Liu, J. H. Ye, B. Ren, Z. L. Yang, Y. Y. Liao, A. See, L. Chan, and Z. Q. Tian, "Raman spectroscopic studies of the formation processes of cobalt silicide thin films," Thin Solid Films **471**, 257 (2005).
14) M. Z. Hasan, G. Chang, I. Belopolski, G. Bian, S.-Y. Xu, and J.-X. Yin, "Weyl, Dirac and high-fold chiral fermions in topological quantum matter," Nat. Rev. Mater. **6**, 784 (2021).
15) G. Chang et al., "Unconventional chiral fermions and large topological Fermi arcs in RhSi," Phys. Rev. Lett. **119**, 206401 (2017).
16) Z. Rao et al., "Observation of unconventional chiral fermions with long Fermi arcs in CoSi," Nature **567**, 496 (2019).
17) P. Tang, Q. Zhou, and S.-C. Zhang, "Multiple types of topological fermions in transition metal silicides," Phys. Rev. Lett. **119**, 206402 (2017).
18) V. Vescoli, L. Degiorgi, B. Buschinger, W. Guth, C. Geibel, and F. Steglich, "The optical properties of RuSi: Kondo insulator or conventional semiconductor?," Solid State Commun. **105**, 367 (1998).
19) H. Hohl, A. P. Ramirez, C. Goldmann, G. Ernst, and E. Bucher, "Transport properties of RuSi, RuGe, OsSi, and quasi-binary alloys of these compounds," J. Alloys Compd. **278**, 39 (1998).
20) B. Buschinger, W. Guth, M. Weiden, C. Geibel, F. Steglich, V. Vescoli, L. Degiorgi, and R. C. Wassilew, "RuSi: metal–semiconductor transition by change of structure," J. Alloys Compd. **262-263**, 238 (1997).
21) K. Breuer, S. Messerli, D. Purdie, M. Garnier, M. Hengsberger, and Y. Baer, "Observation of a gap opening in FeSi with photoelectron spectroscopy," Phys. Rev. B **56**, 7061 (1997).
22) G. Shao, "Thermodynamic analysis of the Re–Si system," Intermetallics **9**, 1063 (2001).

23) Y. Imai, M. Mukaida, K. Kobayashi, and T. Tsunoda, "Calculation of the density of states of transition metal monosilicides by a first-principle pseudopotential method using plane-wave basis," Intermetallics **9**, 261 (2001).
24) D. A. Pshenay-Severin, Y. V. Ivanov, A. T. Burkov, S. V. Novikov, V. K. Zaitsev, and H. Reith, "Electronic structure and thermoelectric properties of transition metal monosilicides," J. Electron. Mater. **47**, 3277 (2018).
25) X. Chen, I. Krivenko, M. B. Stone, A. I. Kolesnikov, T. Wolf, D. Reznik, K. S. Bedell, F. Lechermann, and S. D. Wilson, "Unconventional Hund metal in a weak itinerant ferromagnet," Nat. Commun. **11**, 3076 (2020).
26) V. L. Shaposhnikov, D. B. Migas, V. E. Borisenko, and N. N. Dorozhkin, "Features of the band structure for semiconducting iron, ruthenium, and osmium monosilicides," Semiconductors **43**, 142 (2009).
27) L. F. Mattheiss and D. R. Hamann, "Band structure and semiconducting properties of FeSi," Phys. Rev. B **47**, 13114 (1993).
28) E. G. Moroni, W. Wolf, J. Hafner, and R. Podloucky, "Cohesive, structural, and electronic properties of Fe–Si compounds," Phys. Rev. B. **59**, 12860 (1999).
29) Y. Imai and A. Watanabe, "Electronic structures of platinum group elements silicides calculated by a first-principle pseudopotential method using plane-wave basis," J. Alloys Compd. **417**, 173 (2006).
30) H. Guo-Min, L. Shu-Ping, and H. Mei-Chun, "Structural and electronic properties of RuSi, RuGe and OsSi," Chin. Phys. Lett. **18**, 1389 (2001).
31) N. Acharya and S. P. Sanyal, "Comparative study of structural, electronic and elastic behavior of OsAl and OsSi in B2 and B20 phases under pressure," Indian J. Phys. **91**, 641 (2017).
32) Y. N. Zhao, H. L. Han, Y. Yu, W. H. Xue, and T. Gao, "First-principles studies of the electronic and dynamical properties of monosilicides MSi (M = Fe, Ru, Os)," Europhys. Lett. **85**, 47005 (2009).
33) J. Li, Z. Zhang, Q. Ji, H. Zhang, and H. Luo, "The electronic structure and optical properties of XSi (X = Fe, Ru, Os): a first principles investigation within the modified Becke–Johnson exchange potential plus LDA," J. Alloys Compd. **537**, 297 (2012).
34) D. S. Sanchez et al., "Topological chiral crystals with helicoid-arc quantum states," Nature **567**, 500 (2019).
35) D. A. Pshenay-Severin and A. T. Burkov, "Electronic structure of B20 (FeSi-Type) transition-metal monosilicides," Materials **12**, 2710 (2019).
36) N. G. Galkin, K. N. Galkin, O. V. Kropachev, S. A. Dotsenko, D. L. Goroshko, D. B. Migas, A. B. Filonov, N. V. Skorodumova, A. V. Gerasimenko, and A. K. Gutakovskii, "Ultra-thin and thin CrSi films on Si(111): I. Formation and crystal structure," J. Mater. Chem. C **13**, 2987 (2025).
37) N. G. Galkin, E. Y. Subbotin, K. N. Galkin, D. L. Goroshko, O. A. Goroshko, D. B. Migas, A. B. Filonov, I. A. Tkachenko, and A. Y. Samardak, "Ultra-thin and thin CrSi films on Si(111): II. Transport and magnetic properties," J. Mater. Chem. C **13**, 2875 (2025).
38) N. G. Galkin et al., "New monoclinic ground state of FeSi," Comput. Mater. Sci. **233**, 112762 (2024).
39) K. Göransson, I. Engström, and B. Noläng, "Structure refinements for some platinum metal monosilicides," J. Alloys Compd. **219**, 107 (1995).
40) B. Buschinger, C. Geibel, J. Diehl, M. Weiden, W. Guth, A. Wildbrett, S. Horn, and F. Steglich, "Preparation and low temperature properties of FeSi-type RuSi," J. Alloys Compd. **256**, 57 (1997).
41) B. Buschinger, W. Guth, M. Weiden, C. Geibel, F. Steglich, V. Vescoli, L. Degiorgi, and C. Wassilew-Reul, "RuSi: metal–semiconductor transition by change of structure," J. Alloys Compd. **262-263**, 238 (1997).
42) L. Vočadlo, G. D. Price, and I. G. Wood, "Structures and physical properties of ε-FeSi-type and CsCl-type RuSi studied by first-principles pseudopotential calculations," Acta Cryst. **B56**, 369 (2000).
43) Z. Xiong, X. Wang, L. Cao, J. Wang, J. Yu, H. Yin, X. Wang, and J. Mao, "Structural stability, phase transition, electronic, elastic and thermodynamic properties of RuX (X = Si, Ge, Sn) alloys under high pressure," J. Alloys Compd. **693**, 440 (2017).
44) C. Zhang, Y. Jin, P. Kong, S. Li, S. Chen, W. Zhang, S. Cheng, K. He, and W. Dai, "Theoretical investigations on the structural stability, structural and physical properties, and bonding feature for RuX (X = Si, Ge, Sn) with B20 and B2 phases," Mater. Today Commun. **24**, 101116 (2020).
45) J. A. Hernandez, L. Vočadlo, and I. G. Wood, "High pressure stability of the monosilicides of cobalt and the platinum group elements," J. Alloys Compd. **626**, 375 (2015).
46) K. Schubert, S. Bhan, W. Burkhardt, R. Gohle, H. Meissner, M. Poetzschke, and E. Stolz, "Einige strukturelle ergebnisse an metallischen phasen," Naturwissenschaften **47**, 303 (1960).
47) S. Mozaffari, N. Aryal, R. Schönemann, K.-W. Chen, W. Zheng, G. T. McCandless, J. Y. Chan, E. Manousakis, and L. Balicas, "Multiple Dirac nodes and symmetry protected Dirac nodal line in orthorhombic α-RhSi," Phys. Rev. B. **102**, 115131 (2020).
48) L. Schellenberg, J. L. Jorda, and J. Muller, "The rhodium-silicon phase diagram," J. Less-Common Met. **109**, 261 (1985).
49) G. Kresse and G. J. Hafner, "Ab initio molecular-dynamics simulation of the liquidmetal–amorphous-semiconductor transition in germanium," Phys. Rev. B **49**, 14251 (1994).
50) G. Kresse and J. Furthmüller, "Efficient iterative schemes for ab initio total-energy calculations using a plane-wave basis set," Phys. Rev. B. **54**, 11169 (1996).
51) G. Kresse and J. Joubert, "From ultrasoft pseudopotentials to the projector augmented wave method," Phys. Rev. B. **59**, 1758 (1999).
52) J. Paier, R. Hirschl, M. Marsman, and G. Kresse, "The Perdew–Burke–Ernzerhof exchange-correlation functional applied to the G2–1 test set using a plane-wave basis set," J. Chem. Phys. **122**, 234102 (2005).
53) J. Heyd, G. E. Scuseria, and M. Ernzerhof, "Hybrid functionals based on a screened Coulomb potential," J. Chem. Phys. **118**, 8207 (2003).
54) J. Heyd, G. E. Scuseria, and M. Ernzerhof, "Erratum, hybrid functionals based on a screened Coulomb potential [J. Chem. Phys. 118, 8207 (2003)]," J. Chem. Phys. **124**, 219906 (2006).
55) J. Heyd and G. E. Scuseria, "Assessment and validation of a screened Coulomb hybrid density functional," J. Chem. Phys. **120**, 7274 (2004).
56) J. Heyd and G. E. Scuseria, "Efficient hybrid density functional calculations in solids: assessment of the Heyd–Scuseria–Ernzerhof screened Coulomb hybrid functional," J. Chem. Phys. **121**, 1187 (2004).
57) L. N. Finnie, "Structures and compositions of the silicides of ruthenium, osmium, rhodium and iridium," J. Less-Common Metals **4**, 24 (1962).
58) R. A. McNees and A. W. Searcy, "The crystal structure of rhenium monosilicide," J. Am. Chem. Soc. **77**, 5290 (1955).
59) D. B. Migas, V. L. Shaposhnikov, A. B. Filonov, N. N. Dorozhkin, and V. E. Borisenko, "New semiconducting silicide Ca_3Si_4," J. Phys.: Condens. Matter **19**, 346207 (2007).
60) C.-Z. Zhang, X.-Y. Kuang, Y.-Y. Jin, X.-Z. Yan, and X.-F. Huang, "Structural stability and elastic properties of IrSi in B31 and B20-phase from first-principles calculations," J. Alloys Compd. **585**, 491 (2014).
61) W. Meng, X. Zhang, X. Dai, and G. Liu, "IrSi as a superior electronic material with novel topological properties and nice compatibility with semiconductor Si," Phys. Status Solidi RRL **14**, 2000178 (2020).
62) D. Shiojiri et al., "Re-evaluation of the electronic structure and thermoelectric properties of narrow-gap semiconducting α-$SrSi_2$: a complementary experimental and first-principles hybrid-functional approach," J. Appl. Phys. **129**, 115101 (2021).